Ultrafast Laser Induced Structural Modification of Fused Silica—Part I: Feature Formation Mechanisms

Siniša Vukelić

Panjawat Kongsuwan

Y. Lawrence Yao

Department of Mechanical Engineering,
Columbia University,
New York, NY 10027

Nonlinear absorption of femtosecond-laser pulses enables the induction of structural changes in the interior of bulk transparent materials without affecting their surface. This property can be exploited for transmission welding of transparent dielectrics, three dimensional optical data storages, and waveguides. In the present study, femtosecond-laser pulses were tightly focused within the interior of bulk fused silica specimen. Localized plasma was formed, initiating rearrangement of the network structure. Features were generated through employment of single pulses as well as pulse trains using various processing conditions. The change in material properties were studied through employment of differential interference contrast optical microscopy and atomic force microscopy. The morphology of the altered material as well as the nature of the physical mechanisms (thermal, explosive plasma expansion, or in-between) responsible for the alteration of material properties as a function of process parameters is discussed.
[DOI: 10.1115/1.4002767]

1 Introduction

In recent times, advances in femtosecond-laser development have led to explorations of new applications [1]. One of main advantages of femtosecond lasers in comparison to nanosecond ones is that they induce much less collateral damage due to heat conduction [2]. Furthermore, nonlinear absorption, a unique property of femtosecond lasers, makes them particularly suitable for treatment of dielectric materials [3].

Laser assisted transmission welding using conventional nanoseconond lasers can be utilized when the top material is transparent to the laser and the bottom material is opaque to it [4]. The laser beam transmits trough the top layer and is absorbed by the opaque material beneath. The subsequent heat accumulation helps to create the weld. When using an ultrafast laser, however, nonlinear absorption enables us to induce structural changes in the interior of the target material without affecting the surface and thus the bottom material no longer needs to be opaque. Miyamoto et al. [5] used femtosecond-laser irradiation to simulate fusion welding by inducing damage within the interior of borosilicate glass. Watanabe et al. [6] investigated conditions for joining two substrates using a femtosecond laser. A laser beam was focused on the interface of two transparent substrates resulting in melting and quenching of the surrounding material. Rapid solidification was responsible for joining. Tamaki et al. [7] studied the effect of localized heat accumulation in transmission microwelding. Efforts described above mainly dealt with problems specifically related to welding from a parametric point of view and did not go into details of structural changes that take place within the affected region. To gain insight into the transmission welding process, a more fundamental study of the glass-ultrafast laser interaction is needed. Previous studies on this topic are reviewed in the following paragraph.

The potential of creating three dimensional optical storages [8] has led to the study of the interaction of various transparent materials with ultrafast laser pulses. Glezer and Mazur [9] showed that femtosecond-laser pulses tightly focused into the interior of the glass with an energy level near the threshold produce submicron cavities or voxels. These structures are characterized by a change in refractive index and consist of a centrally placed void accompanied by a denser surrounding region. Bellouard et al. [10] studied the change in morphology of fused silica through its effects on etch selectivity, increase of internal stresses, and densification. Schaffer et al. [11–13] explored different aspects of ultrafast laser fused silica interaction. Topics covered included the potential of micromachining bulk glass with use of nanojoule energy laser pulses, bulk heating of transparent materials, and the morphology of structural changes induced by femtosecond lasers. Kucheyev and Demos [14] used photoluminescence (PL) and Raman spectroscopy to characterize defects created in the amorphous fused silica irradiated by nanosecond and femtosecond lasers with different wavelengths. The induced damage was related to changes in other properties obtained for vitreous silica using different treatments.

The work reviewed above addresses changes in properties and morphology, which are a consequence of structural alterations due to the ultrafast laser irradiation of the interior of transparent materials. It also somewhat explains the physical process that leads to those changes. In the study presented here, the focus is on the contribution of different mechanisms in feature formation under more complex process conditions and much higher laser intensities. In particular, thermal and explosive plasma expansion mechanisms, as well as the transition between the two, are studied.

2 Femtosecond-Laser Irradiation of Transparent Dielectric Materials

In order for interaction to occur between a transparent material and an incident ultrafast laser beam, nonlinear absorption has to take place. The laser energy is deposited into the focal volume and due to short pulse duration, the intensity is high enough to ionize material. Laser induced breakdown [3] then occurs in which the target material in the focal volume is transformed into absorbing plasma with metallic properties. In this way, optically transparent materials become opaque to the incoming laser wavelength as plasma absorbs incoming photons. Further, the plasma is responsible for the damage of the transparent dielectric. Two different

Contributed by the Manufacturing Engineering Division of ASME for publication in the Journal of Manufacturing Science and Engineering. Manuscript received July 27, 2010; final manuscript received August 8, 2010; published online December 17, 2010. Editor: K. F. Ehmann.

Copyright © 2010 by ASME

Downloaded 09 Feb 2011 to 128.59.151.169. Redistribution subject to ASME license or copyright; see http://www.asme.org/terms/Terms_Use.cfm

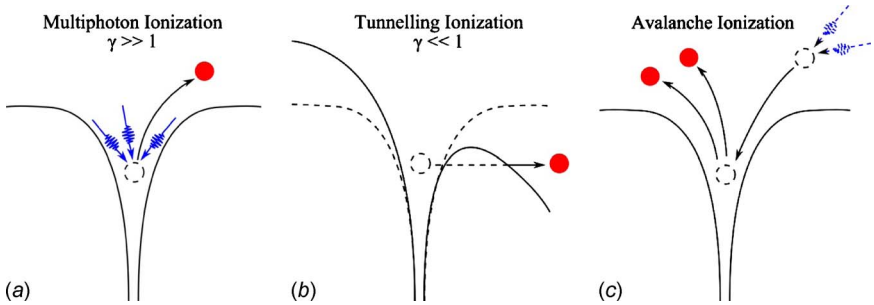

Fig. 1 Schematic diagram of ionization induced by femtosecond-laser irradiation: photoionization as function of Keldysh adiabatic parameter γ: (*a*) multiphoton ionization, (*b*) tunneling ionization, and (*c*) avalanche ionization

mechanisms are known to cause absorption of femtosecond-laser irradiation: photoionization and avalanche ionization [3,11,15,16].

2.1 Photoionization. Photoionization is the process directly initiated by the laser field in which several photons collide with an electron resulting in its excitation. Two regimes are possible depending on the laser frequency and intensity: multiphoton and tunneling ionization. When the laser intensity (photon flux) is above 10^{13} W/cm^2 [3], multiphoton ionization takes place as N photons of same wavelength λ with energy $h\nu$ simultaneously hit a bound electron, as shown in Fig. 1(*a*). If the absorbed energy is greater than the atomic ionization potential ε, the electron is freed from the valence. In the case where the intensity is higher than 10^{15} W/cm^2 [3], the electric field generated by the laser represses the Coulomb well and an electron becomes free by tunneling through deformed valence, as shown in Fig. 1(*b*). Foundations for these processes are laid by Keldysh [15] who established the theory and introduced parameter adiabatic γ, which determines which of two regimes will take place. The parameter γ represents the ratio between the frequency of the laser light ω and the frequency of an electron tunneling through a potential barrier ω_t:

$$\gamma = \frac{\omega}{\omega_t} = \frac{\omega}{e}\sqrt{\frac{mc\varepsilon_0 E_g}{I}} = \frac{1}{2K_0 F} \tag{1}$$

where m is the mass of an electron, c is the speed of light, e is the charge of an electron, n and E_g are the material's refractive index and bandgap, and I is the laser intensity; F represents the reduced electric wave field and K_0 is a process parameter. In the case of a linearly polarized monochromatic wave, the ionization probability in the differential form, w, is given in the following form [15,16]:

$$dw(\boldsymbol{p}) = P\exp(-2K_o(f(\gamma) + c_1(\gamma)q_\parallel^2 + c_2(\gamma)q_\perp^2))\frac{d^3\boldsymbol{p}}{(2\pi)^3} \tag{2}$$

where $P(\gamma)$ is a pre-exponential factor satisfying the assumed conditions $F \ll 1$ and $K_0 \gg 1$, $\boldsymbol{p} = \langle p_\parallel, p_\perp \rangle$ is the photoelectron momentum with components along and perpendicular to the direction of the electric field, $\boldsymbol{q} = \boldsymbol{p}/k$, $f(\gamma)$ is the Keldysh function, and c_1 and c_2 are coefficients describing the photoelectron momentum distribution. In the case of ionization via an ultrashort laser pulse, the coefficients and Kelydish function are

$$f(\gamma) = \int_0^\gamma \chi(u)\left(1 - \frac{u^2}{\gamma^2}\right)du$$

$$c_1(\gamma) = c_2 - \gamma c_2 = \int_0^\gamma (\chi(u) - \chi(\gamma))du$$

$$c_2(\gamma) = \int_0^\gamma \chi(u)du \tag{3}$$

where $\chi(u)$ is a function defined by the shape of the laser pulse. Tunneling ionization takes place when $\gamma \ll 1$. An electron that is originally bound to an atom via a Coulomb well tunnels through the barrier and becomes free as a consequence of the laser induced electric field that suppresses the Coulomb field. At higher laser frequencies ($\gamma \gg 1$) an electron absorbs several quanta simultaneously and gains enough energy to break through the band gap of the material into the free state.

2.2 Avalanche ionization. This type of ionization is active when free electrons produced by multiphoton ionization are heated by the laser pulse and subsequent collisions with the electrons from the valence band results in the generation of multiple free electrons. The process iterates producing a critical density of free electrons in the cloud necessary for plasma formation and the ablation process. Avalanche ionization is schematically represented in Fig. 1(*c*). Collisional ionization is governed by the Fokker–Planck equation [2]:

$$\frac{\partial N(E_K,t)}{\partial t} + \frac{\partial}{\partial E_K}\left[R_J(E_K,t)N(E_K,t) - \alpha(E_K)E_P N(E_K,t) - D(E_K,t)\frac{\partial N(E_K,t)}{\partial E_K}\right] = S(E_K,t) \tag{4}$$

where N is the electron density distribution, E_K is the kinetic energy of an electron, E_P is the phonon energy, t is the time, α is the electron-phonon energy transfer to the lattice, R_J is the electron heating rate, D is the diffusion coefficient, and S represents sources and sinks of electrons. More details about avalanche ionization can be found in Refs. [3,17].

3 Numerical Aperture Dependence on Feature Generation

The nonlinear nature of ultrafast laser pulse absorption enables the structural alteration of internal areas of transparent bulk materials. The mechanism of feature formation is strongly dependent on the way laser energy is deposited into the target material. Schafer et al. [12,13] discussed qualitatively the role of numerical aperture on the nature of structural changes. When laser pulses with energy well above the damage threshold are tightly focused (NA > 0.4) into the transparent material, small regions with large refractive index changes are formed. These regions consist of a hollow or less dense center surrounded by a densified shell. This is a consequence of the explosive expansion of highly energetic plasma created in the focal volume. On the other hand, loose focusing will produce larger affected volume with a smaller re-

Downloaded 09 Feb 2011 to 128.59.151.169. Redistribution subject to ASME license or copyright; see http://www.asme.org/terms/Terms_Use.cfm

fractive index change. Schaffer et al. [12] argued that plasma produced under loose focusing conditions is not energetic enough to create explosive expansion.

Quantification of the focal volume is done primarily in the field of fluorescence correlation spectroscopy (FCS), where nonlinear absorption properties of ultrafast lasers are utilized for imaging the interior of biological systems. The theoretical basis comes from the theory of electromagnetic diffraction in optical systems [17,18].

Electric and magnetic vectors of a monochromatic point source of frequency ω at point P in the object space are as follows:

$$\boldsymbol{E}(P,t) = R\{\boldsymbol{e}(P)e^{-i\omega t}\}$$

$$\boldsymbol{H}(P,t) = R\{\boldsymbol{h}(P)e^{-i\omega t}\} \tag{5}$$

Symbol R denotes the real part. Vectors $\boldsymbol{e}$ and $\boldsymbol{h}$ are generally complex and are the functions of two plane wave functions. It is convenient to define optical coordinates as

$$u = kz \sin^2 \alpha$$

$$v = kr \sin \alpha \tag{6}$$

where $k=2\pi n/\lambda$ is the wave number, λ is the wavelength, and $r^2=x^2+y^2$. The focal plane is located at $u=0$, the longitudinal axis at $v=0$ and in addition to these two parameters the azimuthal angle φ around the longitudinal axis is used as well. From the diffraction theory [17,18], the complex integral representations of electric and magnetic vectors in the image field can be obtained. Energy densities are then defined as

$$\langle w_e(u,v,\phi)\rangle = \frac{1}{8\pi}\langle \boldsymbol{E}^2\rangle = \frac{1}{16\pi}(\boldsymbol{e}\,.\,\boldsymbol{e}*)$$

$$\langle w_m(u,v,\phi)\rangle = \frac{1}{8\pi}\langle \boldsymbol{H}^2\rangle = \frac{1}{16\pi}(\boldsymbol{h}\cdot\boldsymbol{h}^*)$$

$$\langle w(u,v,\phi)\rangle = \langle w_e(u,v,\phi)\rangle + \langle w_m(u,v,\phi)\rangle = \frac{A^2}{8\pi}[|I_o|^2 + 2|I_1|^2 + |I_2|^2] \tag{7}$$

where $\boldsymbol{e}^*$ and $\boldsymbol{h}^*$ denote complex conjugates of electric and magnetic vectors, w_e and w_m are the energy densities of the electric and magnetic fields, respectively, and I_o, I_1, and I_2 are

$$I_0 = \int_0^\alpha \cos^{1/2}\theta \sin\theta(1 + \cos\theta)\cdot J_0(v\sin\theta_P)\exp(ikr\cos\theta\cos\theta_P)d\theta$$

$$I_1 = \int_0^\alpha \cos^{1/2}\theta \sin^2\theta\cdot J_1(v\sin\theta_P)\exp(ikr\cos\theta\cos\theta_P)d\theta$$

$$I_2 = \int_0^\alpha \cos^{1/2}\theta \sin\theta(1-\cos\theta)\cdot J_2(v\sin\theta_P)\times\exp(ikr\cos\theta\cos\theta_P)d\theta \tag{8}$$

where J_i are the Bessel functions of ith order and A is a constant. Integration of the energy density function is the intensity distribution in the vicinity of the focal point that comes from the monochromatic light point source.

4 Experimental Setup and Characterization

An amplified Ti:sapphire laser system (Spectra-Physics Hurricane) with pulse duration of 120 fs at 1 kHz repetition rate and 800 nm wavelength was used to conduct experiments. A Zeiss Plan Neofluar 40× objective lens with a NA of 0.6 was employed to focus the laser, providing approximately a 1.5 μm spot size.

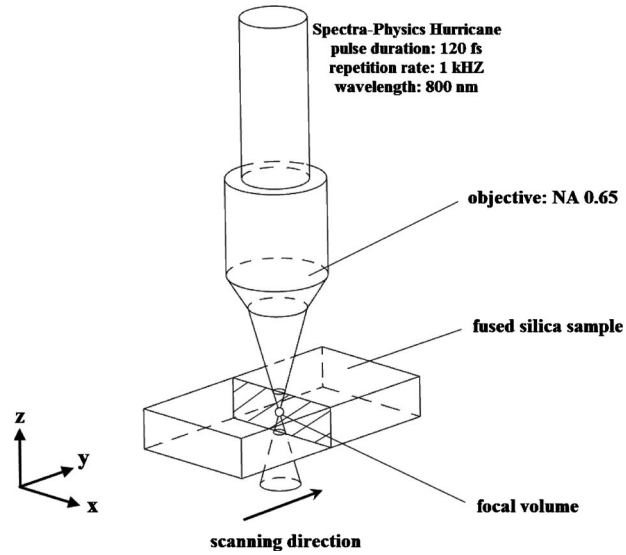

Fig. 2 Schematic illustration experimental setup. The shadowed plane (cross section) shows that the laser beam is focused to the interior of the fused silica sample. Laser beam scanning direction is along y axis.

The beam was focused into the interior of a 1.6 mm thick, 20 mm^2 S1-UV grade fused silica glass specimen mounted on an Aerotech motorized linear stage to create localized structural changes. A schematic diagram of the experimental setup can be seen in Fig. 2. A number of different conditions were applied by varying the feedrate of the stage and the energy of the laser pulses. Pulses were applied at energies ranging from 2 μJ to 35 μJ and stage velocities varied from 0.04 mm/s to 3 mm/s.

Side view optical micrographs were obtained using diffraction interference contrast (DIC) in conjunction with a 1.4 NA oil immersed objective. The sample was then sectioned and polished. In order to preserve perpendicularity between the sectioned plane and the top plane of the specimen, the sample was mounted onto a auxiliary fused silica glass block and two are then polished together. Fused silica glass is chosen for auxiliary block so that both pieces have the same polishing rates. Polishing is done in two stages: First, 1200 grit sand paper was employed to remove cracks due to sectioning. Second, a cerium-oxide powder was applied onto the polishing cloth and paste created by adding distilled water. Specimen is then manually polished. The cross section is observed with transmission optical microscopy. The cross section surface was then mapped using atomic force microscopy (AFM).

5 Results and Discussion

5.1 Feature Morphology and Its Dependence on the Focusing Parameters. In the case when laser pulses with energies well above the damage threshold are deposited into the target material, the morphology of the induced damage is a function of focusing parameters and NA, in particular. Prior to this study, the correlation between NA and the feature morphology has been qualitative. Here an attempt to provide a quantitative correlation between the two is made.

Morphology of the feature created via a single pulse with an energy of 30 μJ can be observed from the side view via DIC optical micrograph, as shown in Fig. 3. The feature appears to be long and narrow with the very bright cylindrical region in the middle. High contrast between the inner region and the surrounding material suggests steep changes in refractive index, which originates from differences in density. Thus it appears that high contrast features are actually voids. Results obtained employing lower energy but still well above damage threshold under two different focusing conditions in borosilicate glass have been re-

Downloaded 09 Feb 2011 to 128.59.151.169. Redistribution subject to ASME license or copyright; see http://www.asme.org/terms/Terms_Use.cfm

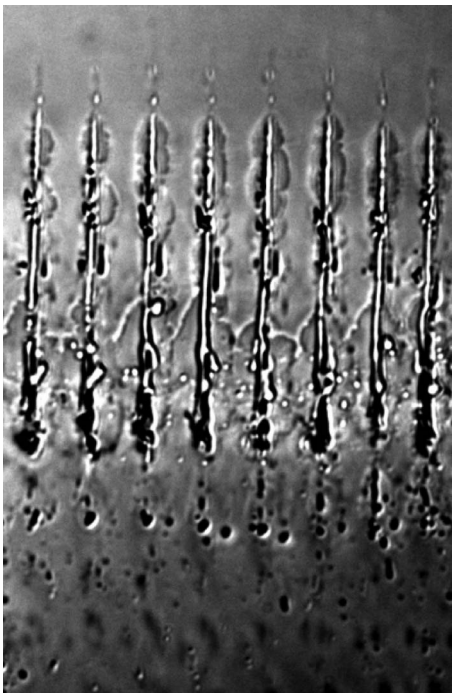

Fig. 3 DIC optical microscope side view (y-z plane) of features created via single femtosecond-laser pulses in fused silica sample. Pulse energy is 30 μJ.

ported by Schaffer et al. [13].

Laser intensity in the vicinity of the focal point can be calculated through employment of the of an illumination point spread function (IPSF), which comes from the work of Richards and Wolf [18]. From energy density expressed by Eq. (7), longitudinal and lateral radii of the focal volume can be obtained. Hess and Webb [19] obtained estimates of the radii assuming that the focal volume has the shape of a Gaussian ellipsoid:

$$\omega_z = \frac{0.532\lambda}{\sqrt{2}}\left(\frac{1}{n-\sqrt{n^2-NA^2}}\right)$$

$$\omega_{xy} = \frac{0.32\lambda}{\sqrt{2}NA}, NA \leq 0.7$$

$$\omega_{xy} = \frac{0.325\lambda}{\sqrt{2}NA^{0.91}}, NA > 0.7 \tag{9}$$

where n is the refractive index. Taking into account the assumption that the affected volume is proportional to the focal volume, one can compare the ratios of longitudinal and lateral radii calculated from Eq. (9) and those obtained experimentally. This comparison is shown in Fig. 4, where experimental findings include features generated by Schaffer et al. [13] with 500 nJ pulse energy and NAs of 0.45 and 1.2, respectively, and ours, which are produced with 30 μJ pulse energy and 0.6 NA. The figure suggests that the proposed estimates are in good agreement. The theoretical prediction underestimates the ratio of the features radii created with 500 nJ pulse energy in borosilicate glass, whereas the ratios of the features produced with pulses of 30 μJ energy in fused silica are slightly smaller than the theoretical estimate. Also it should be noted that the discrepancy becomes smaller as the NA increases. Also, although the ratios are close, the theoretically predicted major and minor radii of the focal volume ellipsoid are ten times smaller than the radii of the affected volume observed experimentally. This is indicative that the focal and affected volumes are indeed in proportion.

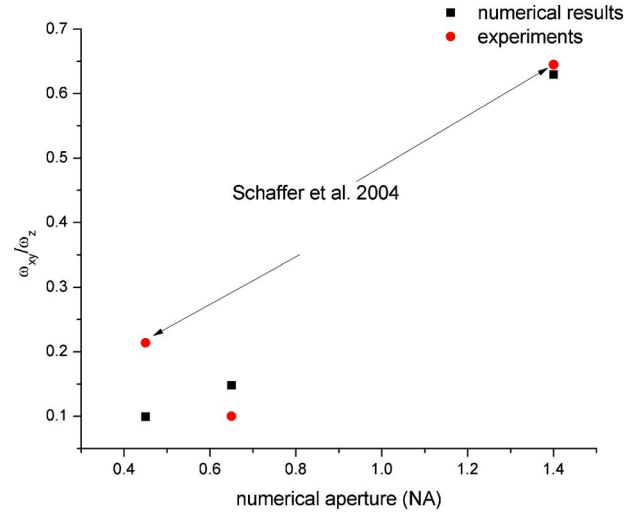

Fig. 4 Comparison between numerical and experimental observations of focal and affected volume longitudinal and lateral radius ratio

5.2 Structural Changes Produced via Line of Overlapping Pulses. Figure 5 shows a cross section of the femtosecond irradiated fused silica sample. Ten different sets of energy levels starting from 2 μJ at the far left to 35 μJ at the right side have been introduced into the specimen interior. Within each set there are 12 different scanning speeds from 0.04 mm/s to 1 mm/s. The distance between adjacent lines is about 35 μm and there is no interference between treated regions. It can also be seen that the structural modifications induced are within the interior of the sample about 400 μm away from the top surface and the material between the surface and the features is not affected. Figures 6(*a*) and 6(*b*) depict cross sections of the features produced with 30 μJ laser pulse energy at various feedrates and ones made at a 1 mm/s feedrate with different pulse energies, respectively.

These features display a teardrop shape, as shown in Fig. 6(*a*), similar to those observed elsewhere [5]. The shape of the features can be attributed to the geometry of the focal volume, which follows the Gaussian ellipsoid. From Fig. 6(*a*), it can also be seen that at this fixed pulse energy level, the feature width is strongly dependent on the scanning speed which is proportional to the amount of overlapping between pulses. A similar conclusion can be drawn for the case when the feedrate is fixed and the pulse energy is varied, as shown in Fig. 6(*b*).

At lower feedrates, two regions within the feature can be dis-

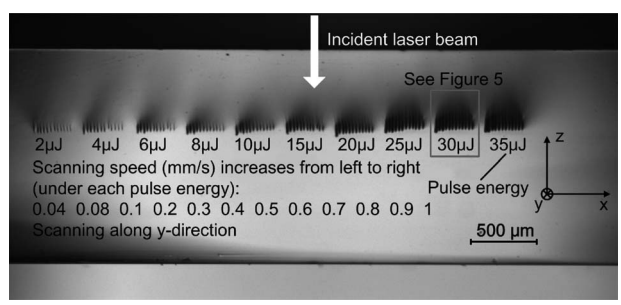

Fig. 5 Optical microscopy of cross section view (x-z plane) of femtosecond-laser-irradiated fused silica at different energy levels (from 2 μJ up to 35 μJ) and scanning speeds (from 0.04mm/s up to 1mm/s for each energy level). Scanning is along the y direction, perpendicular to the cross section x-z plane. In order to improve the image quality, the sample was diced and polished after experiment. The rectangle region of 30 μJ pulse energy is magnified in Fig. 6(*a*).

Downloaded 09 Feb 2011 to 128.59.151.169. Redistribution subject to ASME license or copyright; see http://www.asme.org/terms/Terms_Use.cfm

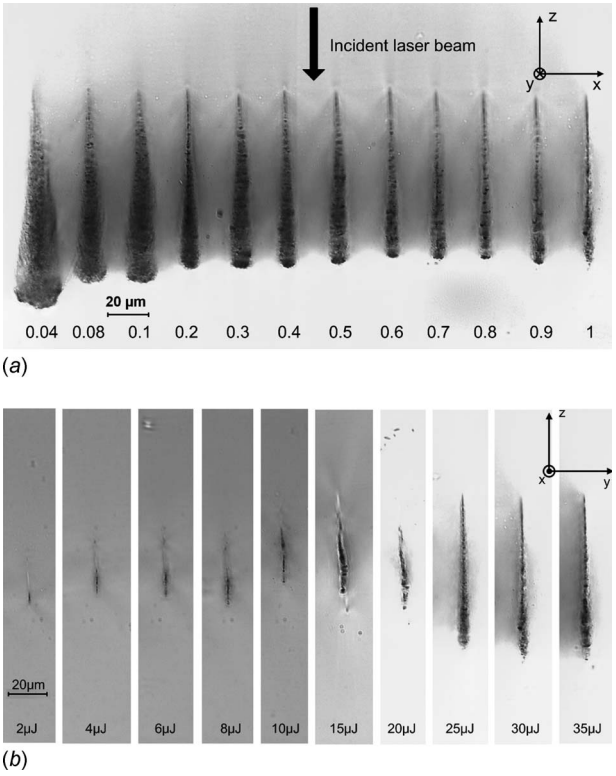

Fig. 6 Optical microscopy of cross section view (x-z plane) of femtosecond-laser-irradiated fused silica sample: (*a*) energy level of 30 μJ with various scanning speeds, (*b*) feedrate 1 mm/s and different energy levels; both extracted from Fig. 5

tinguished [5]. The inner region corresponds to the material melted within the focal volume [12], which is based on the assumption that femtosecond-laser energy deposited within the focal volume at low stage velocities behaves as a moving heat source. The formation of the outer region is a consequence of heat conduction between the inner region and surrounding material. At higher feedrates, the feature is much narrower, and instead of a relatively broad inner region, only a sharp line in the middle of the teardrop is observed. One explanation is that as the stage speed increases, the amount of overlapping decreases, and as a result, the feature generating mechanism is less thermal in nature. The amount of heat transfer between the focal volume and surrounding area decreases resulting in a narrower feature. Further, explosive plasma expansion upon a single femtosecond-laser pulse creates voids surrounded by densified material [11,12]. When overlapping is not significant, explosive plasma expansion mechanism might be responsible for the feature generation. This implies that the sharp lines in the middle of the features observed at higher scanning speeds are actually voids. This will be shown in Secs. 5.3 and 5.4.

Figure 7 shows the width to height ratio of these interior features as a function of feedrate. Note that at each feed rate, there are ten energy levels and their effect on the ratio is represented by an error bar. Three regions attributed to the mechanism responsible for the feature formation are observed. The ratio between lateral and longitudinal radii decreases from lower feed rates (where the thermal mechanism dominant) to higher feed rates (where the explosive plasma expansion mechanism dominant). With the medium feed rates, both mechanisms co-exist. This trend is understandable as the low feed rates lead to more overlapping and thus the thermal mechanism dominates. As a result, the feature is widened and the ratio increases. At high feed rates, there is less overlapping and thus the explosive plasma expansion dominates. As a result, the ratio at high feed rates more or less follows

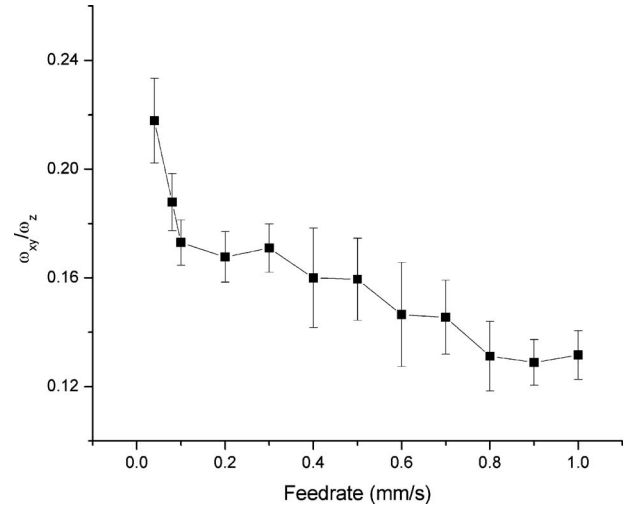

Fig. 7 Experimental measurement of ratio between lateral and longitudinal radii of affected volume. Error bars represent standard deviation.

Eq. (9) and is equal to about 0.15, as seen in Fig. 4 for NA =0.65 used in this study. Please note the effect of feed rate on the ratio that is more pronounced than that of the energy level. In other word, overlapping plays a major role in determining which mechanism is more dominant.

5.3 Discussions of the Mechanisms Responsible for Feature Generation and the Periodic Nature of the Induced Structures. In addition to the analysis above, more detailed one is presented here based on side-view micrographs. The features produced in the bulk specimen with overlapping laser pulses appear to have the shape of the continuous line. However, its structure at higher feedrates are rather periodic. Figure 8 shows side views of femtosecond-laser generated features in the interior of samples captured using transmission DIC optical microscopy. Three different conditions are shown in the figure, created with the same laser pulse energy (30 μJ), but different feedrates, 1 mm/s, 0.5 mm/s, and 0.04 mm/s, respectively. The slight discrepancy in feature size between the cross section and side views comes from the fact that at high magnification, the depth of field of objectives is very small and since the feature is three dimensional it is possible to focus on a fraction of its size. All the structures are formed using laser energy orders of magnitude above the threshold intensity with tight focusing, which implies creation of cavities within the focal volume.

Figure 8(*a*) shows the case with 1 mm/s feedrate. Here there is 33% (repetition rate of 1 kHz and approximate beam spot size 1.5 μm) overlapping between consecutive pulses, which lead to complicated morphology. Two distinctive regions can be seen: The lower of which corresponds to the wider portion of the teardrop shape in cross section and the upper one corresponds to the tail of the teardrop. Similar to the single pulse features, as shown in Fig. 3, narrow, elongated, bright regions can be seen. These are regions of very different refractive indices and are probably voids. At the lower portion of the affected area, the material appears to be cracked. It is also observed that the cylindrical bright regions are highly irregular, which is a consequence of the overlapping of laser pulses. A single pulse creates a void and alters the structure of the irradiated material and therefore, the subsequent pulse hits already modified material that contains voids.

A sample for which the stage feedrate was lowered to 0.5 mm/s is shown in Fig. 8(*b*). Here it can be seen that toward the lower edge of the affected zone, the material appears to be homogeneously altered, possibly through a thermal mechanism. The intermediate zone has contrast similar to the untreated region suggest-

Downloaded 09 Feb 2011 to 128.59.151.169. Redistribution subject to ASME license or copyright; see http://www.asme.org/terms/Terms_Use.cfm

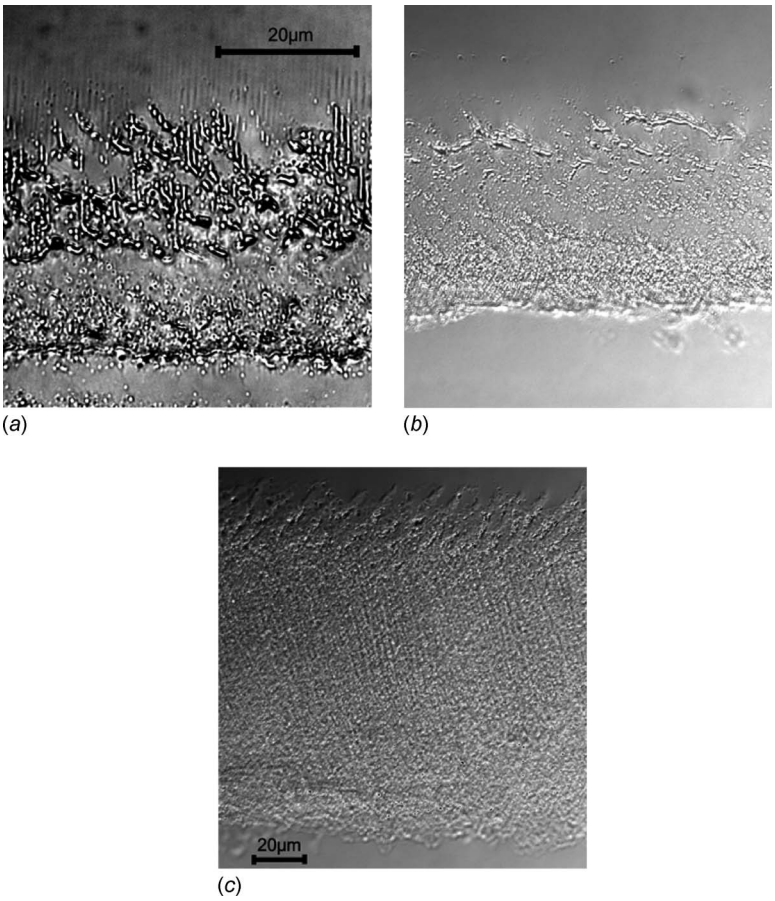

Fig. 8 DIC optical microscope side view (y-z plane) of femtosecond-laser-irradiated fused silica sample at energy level of 30 μJ with three different scanning speeds: (*a*) with scanning speed of 1 mm/s, (*b*) with scanning speed of 0.5 mm/s, and (*c*) with scanning speed of 0.04 mm/s. Images are taken using (*a*) 100× and ((*b*) and (*c*)) 40× oil immersed objective lenses.

ing that there is not much refractive index change and it is filled with bubblelike features, which might be very small voids. In the tailing edge of the feature (upper portion), crack formation is observed. As feedrate is reduced, transition between explosive plasma explosion and thermal accumulation occurs, manifested through change in morphology and reduction of the voids. This is probably a result of both gradual build-up of thermal accumulation and influence of subsequent pulse hits on already altered material. In addition, this interesting phenomenon, which is to the authors' best knowledge observed for the first time, will be subject of future studies.

At the slowest stage velocity, as shown in Fig. 8(*c*), the feature is quite homogeneous and appears to be created via melting and rapid resolidification. The change in contrast between the affected region and the surrounding material is not as pronounced and thus the refractive index alteration is smaller than in the densified area present in the case of explosive plasma explosion.

If we assume that the laser intensity at a certain spatial position follows the Gaussian distribution of the laser beam waist, in the case of a 1 mm/s feedrate, due to the partial overlapping of the laser pulses, the pitch is about 1 μm, which corresponds to the distance between the dark lines above the cavity area. Due to the superposition of the intensities produced by the laser pulses, there is a threshold intensity that every point in the laser path receives. With a decrease of scanning speed, this threshold increases and the spikes, which are a consequence of the Gaussian intensity distribution, decrease, leaving the spatial distribution of energy received by the sample flat. Furthermore, the total amount of energy received by a point on the laser path increases significantly from a 33% overlap between pulses to a 95% overlap. For a 1 mm/s feedrate, spiked regions receive the least pulse overlapping and that is where cavities are likely to be formed.

5.4 Voids Creation in the Inner Region. As discussed in Sec. 5.3, at higher feedrates the mechanism responsible for feature generation is explosive plasma expansion. This mechanism is athermal in nature and as a result it creates cavities surrounded by densified material within the interior of bulk specimen. If overlapping between pulses is smaller than a certain critical threshold, the above mechanism will apply and femtosecond-laser pulses will generate cavities. Figure 9 shows the cross sectional area of the fused silica sample scanned via AFM. Features shown are created with 30 μJ laser pulse energy and feedrates ranging from 1.0 mm/s to 0.6 mm/s. Other conditions have been scanned as well but they have not revealed presence of the cavities, which supports the hypothesis of the thermal nature of the structure formation at lower feedrates.

From the Fig. 9, it can be seen that laser pulses actually created trains of cavities along the longitudinal axis of the feature, corresponding to the features seen on the DIC side-view optical micrographs. Several different sections have been scanned and trains of cavities have been observed in most of them. The affected region is slightly depressed with respect to the untreated material and that is probably due to the different polishing rate of the material altered by the laser irradiation, so a teardrop shape similar to those observed in the cross section optical micrographs can be seen in

Downloaded 09 Feb 2011 to 128.59.151.169. Redistribution subject to ASME license or copyright; see http://www.asme.org/terms/Terms_Use.cfm

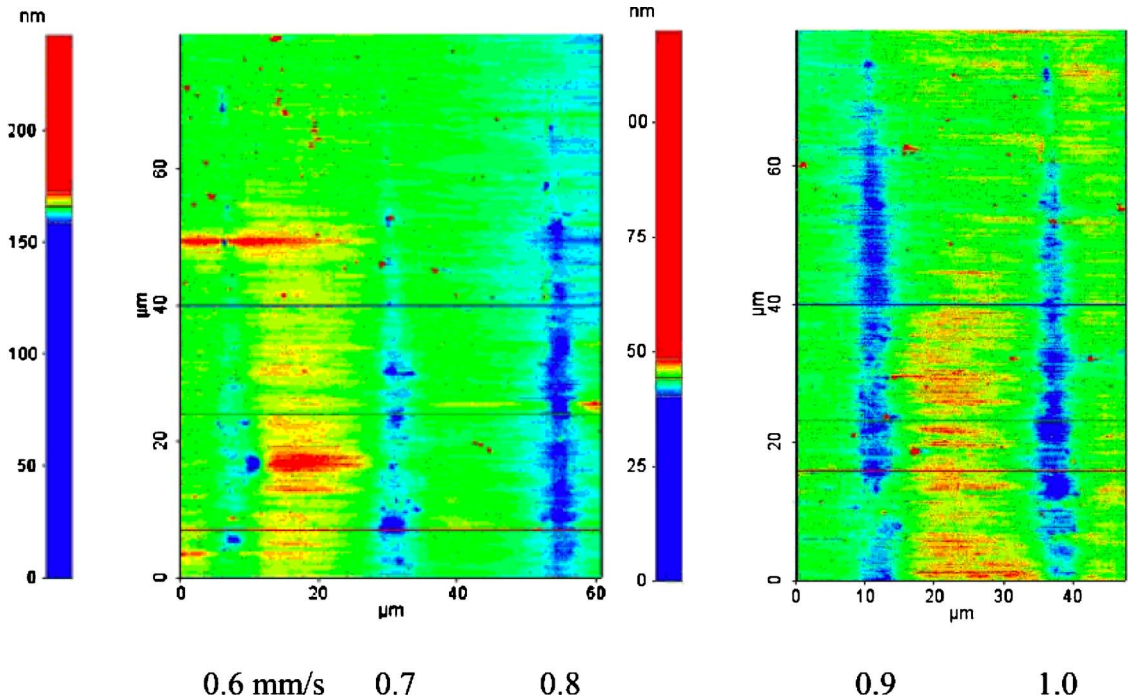

Fig. 9 AFM cross section (x-z plane) topography of laser-irradiated fused silica sample. The five lines (from left to right) shown in the figure correspond to three different experimental regimes, scanning speeds from left to right 0.6, 0.7, 0.8, 0.9, and 1.0 mm/s with the same 30 μJ pulse energy.

AFM scans as well. As feedrate decreases at constant laser pulse energy, the size of the cavities decreases. Due to the periodic nature of the generated structures, it is not meaningful to quantitatively compare depths of the features because they are dependent on the cross section and it is practically impossible to precisely control the sectioning of the sample. However, it should be noted that the maximum depth of the cavities decrease with decrease in feedrate leading to the total absence of voids at stage velocities lower than 0.6 mm/s, as seen in Fig. 10.

6 Conclusion

The interior of amorphous fused silica was subjected to ultrafast laser irradiation with pulse energies higher than the threshold for multiphoton/avalanche ionization. The morphology of the structural alteration created via a single pulse as well as a number of partially overlapping laser pulses, which form pulse trains with different federates, has been investigated. To quantitatively investigate the single pulse response, the electromagnetic diffraction theory of optical systems has been employed. The focal volume size, obtained from the illumination point spread function, is compared with experimental findings in terms of lateral and longitudinal radii and a qualitative agreement is seen. Further, in the case when pulse trains were used for feature generation, two different mechanisms (thermal and explosive plasma expansion) based on process conditions have been explored and potential explanation for transition between two regimes given. It is concluded that pulse energy has a dominant influence on the feature size, whereas feedrate is predominantly responsible for the type of mechanism that will take place. Irregular cavity formation in the form of trains in the regime when partial overlapping takes place is observed via DIC optical micrographs and AFM. This phenomenon is likely to occur due to the interaction between voids, as well as the different responses of the material that has already been altered by a previous pulse.

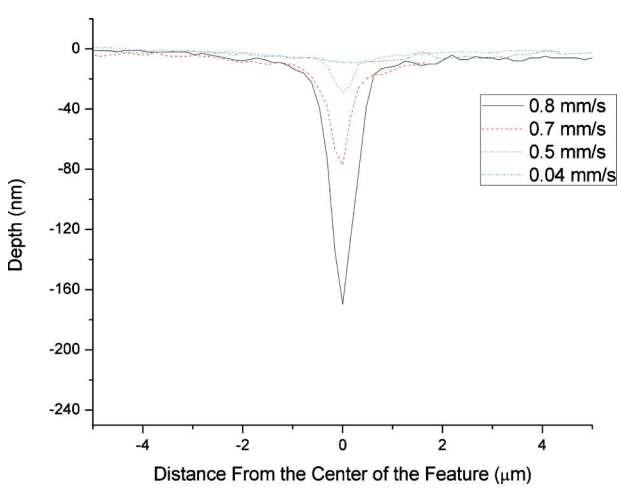

Fig. 10 Maximum depth of the cavities found via AFM topography of the cross section. Voids are created by the 30 μJ pulse energy at different feedrates. The comparison is qualitative and similar trend is observed at various cross section.

Acknowledgment

The authors would like to thank Professor John R. Lombardi of the City University of New York and Dr. Tommaso Baldacchini of Newport/Spectra-Physics for useful discussions. Assistance in preparing figures by Mr. Haohao Jiao is also gratefully acknowledged.

References

[1] Shirk, M. D., and Molian, P. A., 1998, "A Review of Ultrashort Pulsed Laser Ablation of Materials," J. Laser Appl., **10**(1), pp. 18–28.

[2] Stuart, B. C., Feit, M. D., Rubenchik, A. M., Shore, B. W., and Perry, M. D., 1995, "Laser-Induced Damage in Dielectrics With Nanosecond to Subpicosecond Pulses," Phys. Rev. Lett., **74**(12), pp. 2248–2251.

[3] Jiang, L., and Tsai, H. L., 2003, "Femtosecond Lasers Ablation: Challenges and Opportunities," NSF Workshop on Unsolved Problems and Research Needs in Thermal Aspects of Material Removal Processes, Stillwater, OK.

Downloaded 09 Feb 2011 to 128.59.151.169. Redistribution subject to ASME license or copyright; see http://www.asme.org/terms/Terms_Use.cfm

[4] Tan, A. W. Y., and Tay, F. E. H., 2005, "Localized Laser Assisted Eutectic Bonding of Quartz and Silicon by Nd-YAG Pulsed-Laser," Sens. Actuators, A, **120**, pp. 550–561.
[5] Miyamoto, I., Horn, A., Gottmann, J., Wortmann, D., and Yoshino, F., 2006, "High-Precision, High-Throughput Fusion Welding of Glass Using Femtosecond Laser Pulses," Proceedings of the Fourth International Congress on Laser Advanced Materials Processing, Kyoto Research Park, Kyoto, Japan.
[6] Watanabe, W., Onda, S., Tamaki, T., and Itoh, K., 2007, "Direct Joining of Glass Substrates by 1 kHz Femtosecond Laser Pulses," Appl. Phys. B: Lasers Opt., **87**, pp. 85–89.
[7] Tamaki, T., Watanabe, W., Nishii, J., and Itoh, K., 2005, "Welding of Transparent Materials Using Femtosecond Laser Pulses," Jpn. J. Appl. Phys., Part 2, **44**(22), pp. L687–L689.
[8] Glezer, E. N., Milosavljevic, M., Huang, L., Finlay, R. J., Her, T.-H., Callan, J. P., and Mazur, E., 1996, "Three-Dimensional Optical Storage Inside Transparent Materials," Opt. Lett., **21**(24), pp. 2023–2025.
[9] Glezer, E. N., and Mazur, E., 1997, "Ultrafast-Laser Driven Micro-Explosions in Transparent Materials," Appl. Phys. Lett., **71**(7), pp. 882–884.
[10] Bellouard, Y., Colomb, T., Depeursinge, C., Said, A. A., Dugan, M., and Bado, P., 2006, "Investigation of Femtosecond Laser Irradiation on Fused Silica," Proc. SPIE, **6108**, pp. 155–160.
[11] Schaffer, C. B., Brodeur, A., Garcia, J. F., and Mazur, E., 2001, "Micromachining Bulk Glass by Use of Femtosecond Laser Pulses With Nanojoule Energy," Opt. Lett., **26**(2), pp. 93–95.
[12] Schaffer, C. B., Garcia, J. F., and Mazur, E., 2003, "Bulk Heating of Transparent Materials Using a High-Repetition-Rate Femtosecond Laser," Appl. Phys. A: Mater. Sci. Process., **76**, pp. 351–354.
[13] Schaffer, C. B., Jamison, A. O., and Mazur, E., 2004, "Morphology of Femtosecond Laser-Induced Structural Changes in Bulk Transparent Materials," Appl. Phys. Lett., **84**(9), pp. 1441–1443.
[14] Kucheyev, S. O., and Demos, S. G., 2003, "Optical Defects Produced in Fused Silica During Laser-Induced Breakdown," Appl. Phys. Lett., **82**(19), pp. 3230–3232.
[15] Keldysh, L. V., 1965, "Ionization in the Field of a Strong Electromagnetic Wave," Sov. Phys. JETP, **20**(5), pp. 1307–1314.
[16] Popov, V. S., 2004, "Tunnel and Multiphoton Ionization of Atoms and Ions in a Strong Laser Field (Keldysh Theory)," Phys. Usp., **47**(9), pp. 855–885.
[17] Wolf, E., 1959, "Electromagnetic Diffraction in Optical Systems. I. An Integral Representation of the Image Field," Proc. R. Soc. London, Ser. A, **253**(1274), pp. 349–357.
[18] Richards, B., and Wolf, E., 1959, "Electromagnetic Diffraction in Optical Systems. II. Structure of the Image Field in an Aplanatic System," Proc. R. Soc. London, Ser. A, **253**(1274), 358–379.
[19] Hess, S. T., and Webb, W. W., 2002, "Focal Volume Optics and Experimental Artifacts in Confocal Fluorescence Correlation Spectroscopy," Biophys. J., **83**, pp. 2300–2317.

Downloaded 09 Feb 2011 to 128.59.151.169. Redistribution subject to ASME license or copyright; see http://www.asme.org/terms/Terms_Use.cfm